Determination of Fe−Ligand Bond Lengths and the Fe−N−O Bond Angles in Soybean Ferrous and Ferric Nitrosylleghemoglobin *a* Using Multiple-Scattering XAFS Analyses[†]

Anne M. Rich,[‡] Paul J. Ellis,[‡] Linda Tennant,[§] Peter E. Wright,[§] Robert S. Armstrong,[‡] and Peter A. Lay*[,‡]

School of Chemistry, University of Sydney, New South Wales, 2006 Australia, and Department of Molecular Biology, Research Institute of Scripps Clinic, 10550 North Torrey Pines Road, La Jolla, California 92037

Received March 30, 1999; Revised Manuscript Received August 16, 1999

ABSTRACT: The NO adducts of leghemoglobin (Lb) are implicated in biological processes, but only the adduct with ferrous Lb ($Lb^{II}NO$) has been characterized previously. We report the first characterization of ferric nitrosylleghemoglobin ($Lb^{III}NO$) and XAS experiments performed on frozen aqueous solutions of $Lb^{II}NO$ and $Lb^{III}NO$ at 10 K. The XANES and electronic spectra of the NO adducts are similar in shape and energies to the myoglobin (Mb) analogues. The environment of the Fe atom has been refined using multiple-scattering (MS) analyses of the XAFS data. For $Lb^{II}NO$, the MS analysis resulted in an averaged Fe−N_p(pyrrole) distance of 2.02 Å, an Fe−N_ϵ(imidazole) distance of 1.98 Å, an Fe−N_{NO} distance of 1.77 Å, and an Fe−N−O angle of 147°. The Fe−N_{NO} distance and Fe−N−O angle obtained from the analysis of $Lb^{II}NO$ are in good agreement with those determined crystallographically for [Fe(TPP)(NO)] (TPP, tetraphenylporphyrinato), with and without 1-methylimidazole (1-MeIm) as the sixth ligand, and the MS XAFS structures reported previously for the myoglobin ($Mb^{II}NO$) analogue and [Fe(TPP)(NO)]. The MS analysis of $Lb^{III}NO$ yielded an average Fe−N_p distance of 2.00 Å, an Fe−N_ϵ distance of 1.89 Å, an Fe−N_{NO} distance of 1.68 Å, and an Fe−N−O angle of 173°. These bond lengths and angles are consistent with those determined previously for the myoglobin analogue ($Mb^{III}NO$) and the crystal structures of the model complexes, $[Fe^{III}(TPP)(NO)(OH_2)]^+$ and $[Fe(OEP)(NO)]^+$ (OEP, octaethylporphyrinato). The final XAFS *R* values were 16.1 and 18.2% for $Lb^{II}NO$ and $Lb^{III}NO$, respectively.

Leghemoglobin (Lb)[1] (*1*−*4*) is a small (16−17 kDa) protein that facilitates the transport of O_2 to respiring N_2-fixing bacteria at concentrations of free O_2 too low to inactivate nitrogenase (*3*). Although the structure of Lb is similar to that of myoglobin (Mb), Lb has a much higher affinity for O_2, principally because the association rate is 10−20 times higher (*3*). The more accessible distal cavity in Lb versus Mb is also reflected in the binding of bulky ligands such as propionate, butyrate, valerate, and nicotinate (*5*, *6*), which bind to met-Lb almost as freely as does acetate, but not to met-Mb (*3*). The NO adducts of Lb may have a physiological role in the control of N_2 fixation, since nitrate is a known physiological inhibitor of nitrogenase activity, which might be exerted through its reduction to nitrite (*3*). In vivo, nitrite is reduced in the presence of Lb to form nitrosyl Lbs (*7*), which inhibits their ability to bind O_2.

Most solution studies of Lb have used Lb *a* from soybean (*Glycine max*), while most of the XRD studies have used Lb II from yellow lupin (*Lupinus luteus*) (*7*−*10*). While these proteins are distant on the phytogenetic tree (*11*) and differ significantly in length (Lb *a* has 143 residues, Lb II has 153 residues), when their sequences are aligned, they have identical residues at 82 positions (57% sequence identity). The four major (Lb *a*, Lb c_1, Lb c_2, and Lb c_3) and four minor components (Lb *b*, Lb d_1, Lb d_2, and Lb d_3) of soybean Lb (*12*, *13*) all have similar amino acid sequences (*11*, *12*), ligand-binding constants (*2*, *12*, *14*), electronic spectral properties (*14*), and EPR spectra (*15*).

Resonance Raman (RR) (*16*) and NMR (*17*) spectroscopic studies of low-spin O_2, CO, NO, and RNC adducts of ferrous Mb and Lb and Lb(II)−nicotinate (*16*, *18*−*20*) suggest a more constrained heme structure and stronger ligand field at the Fe atom of soybean Lb as compared to Mb or Hb. It was proposed that heme ruffling in Lb rather than changes in Fe−histidine bonding leads to strengthening of the ligand field.

RR spectra from NO adducts of a range of heme proteins indicate a bent Fe−N−O moiety for the Fe(II) adduct and a

[†] We are grateful for funding from the Major Facilities Program funded by the Department of Industry, Science and Resources and managed by the Australian Nuclear Science and Technology Organisation, an Australian Postgraduate Research Award, and James Kentley Memorial Traveling Scholarship (A.M.R.) and the Australian Research Council (R.S.A. and P.A.L.). Work was done (partially) at SSRL, which is operated by the Department of Energy, Office of Basic Science. The SSRL Biotechnology Program is supported by the NIH, Biomedical Research Technology Program, National Center for Research Resources. Further support is provided by the Department of Energy, Office of Health and Environmental Research.

* Corresponding author. Tel: 61-2-9351-4269. Fax: 61-2-9351-3329. E-mail: lay_p@chem.usyd.edu.au.

[‡] University of Sydney.

[§] Research Institute of Scripps Clinic.

[1] Abbreviations: cyt *c*, cytochrome *c*; Hb, hemoglobin; KP_i, potassium phosphate buffer; Lb, leghemoglobin; Mb, myoglobin; MS, multiple scattering; OEP, octaethylporphyrinato(2−); P450cam, the *d*-camphor-bound form of cytochrome P450 from *Pseudomonas putida*; P450nor-NO, nitric oxide reductase (nor) enzyme from *Fusarium oxysporum*; RR, resonance Raman; sGC, soluble guanylyl cyclase; SS, single scattering; TPP, tetraphenylporphyrinato(2−).

10.1021/bi990730n CCC: $18.00
Published on Web 11/23/1999

linear Fe−N−O moiety, with an Fe(II)−NO^+ electronic structure, for the Fe(III) adduct (*21*−*26*). The XRD and single-scattering (SS) XAFS structural information on NO adducts of heme proteins is confined to XAFS analysis of sperm whale $Mb^{II}NO$ (*27*) and to the X-ray crystal structures of horse $Hb^{II}NO$ (*28*), RSNO−$Hb^{II}NO$ (*29*), lupin $Lb^{II}NO$ (*9, 10*), sperm whale $Mb^{II}NO$ (*30*), and the NO adduct of cyt *c* peroxidase (*31*).

The errors in bond lengths and angles in the available XRD structures are expected to be relatively large (>0.1 Å in bond lengths even for the highest resolution 1.7 Å structures). In contrast, MS XAFS analyses can determine Fe−L bond lengths accurate to 0.01−0.03 Å (*32*). The use of MS XAFS analysis and restrained and constrained bond angles and distances for heme proteins and porphyrins has been described in detail in the early 1990s (*33*−*35*). More recently, MS XAFS determinations of Fe−N−O bond angles in non-heme Fe complexes (*36*), $Mb^{II}NO$ and $Mb^{III}NO$ (*37*), and nitric oxide reductase (*23*) have been reported.

MS XAFS analyses were undertaken to (i) obtain more accurate Fe−ligand bond length and Fe−N−O bond angle data than those obtained from XRD of $Lb^{II}NO$ (*9, 10*); (ii) obtain information on the previously unreported $Lb^{III}NO$; and (iii) compare the resulting structures with the analogous MbNO adducts (*37*).

EXPERIMENTAL PROCEDURES

General Procedures. Proteins were handled using protein-clean glassware that was soaked overnight in dilute RBS 35 (Stansens Scientific) solution followed by concentrated nitric acid (15 M), Na_2H_2EDTA solution (0.1 M), and Milli-Q water.

Protein solutions were stored at 4 °C, or for storage of >1 week, samples were frozen in the stable, ferric form (*19*) in screw-capped vials and stored in liquid N_2. The absorption ratio of thawed and repurified Lb *a* was measured to check for denaturation (A_{Soret}/A_{280} = 5.4; >5.0 for met-Lb is considered acceptable) (*14*). AR reagents were used for buffer preparations, and Milli-Q water was used to prepare all solutions.

Electronic spectra were recorded using a Cary 5E UV−visible-NIR spectrophotometer, (∼20 °C, 0.5-nm resolution, scan rate of 900 nm/min) or a Hewlett-Packard 8452A diode array spectrophotometer (∼20 °C, 2-nm resolution) for samples used for the XAFS analyses (after 1000-fold dilution). Spectra were recorded for $Lb^{II}NO$ and $Lb^{III}NO$ periodically during the preparations to examine the extent of ligation and after their exposure to the X-ray beam to monitor any degradation of the protein. Protein samples were concentrated using a Sorvall RC-5B refrigerated superspeed centrifuge (Du Pont) and SS-34 rotor (8000 rpm; 2−4 °C) or a Beckman-GPKP centrifuge and SS-34 rotor (8000 rpm; 2−4 °C, SSRL).

Purification of Protein (11). Crude soybean Lb *a* was dialyzed against a Tris buffer solution (0.1 M Tris-HCl, pH 7.7, 0.0001 M EDTA) and then concentrated using an Amicon concentrator and a YM-10 membrane (Millipore). A solution of Lb (∼9−11 mM) was oxidized with a 10-fold excess of solid $K_3[Fe(CN)_6]$ (Fisher, ACS reagent). $[Fe(CN)_6]^{3-/4-}$ and any other small molecular weight species were removed using a Sephadex G-15 column preequilibrated with Tris-HCl (0.01 M, pH 9.2, 5 °C). The pooled fractions were then concentrated on a YM-10 filter, and the buffer was changed to AcH/NaAc (0.01 M, pH 5.2). The Lb acetate solution was loaded onto an AcH/NaAc-equilibrated DE-52-cellulose (Whatman) column, and four bands were eluted in the following order: Lb *a*, Lb *b*, Lb *c*, Lb *d*. Using an Amicon and a YM-10 filter, the pooled Lb *a* fractions were buffer-exchanged to KH_2PO_4/K_2HPO_4 (0.01 M, pH 7.0) and concentrated to a volume of 1.0 mL (∼10 mM).

NO Adducts. Nitrogen dioxide was removed from NO (C.I.G. Matheson, certified >99%) by bubbling it through 1 M NaOH (*21*, *26*, *38*). A sample of $Lb^{II}NO$ in KP_i (0.1 M, pH 7.0) was prepared by reduction of met-Lb with $Na_2S_2O_4$ dissolved in 10 mM NaOH to guard against a change in pH.[2] To ensure complete reduction to deoxy-Lb, a 10-fold excess of $Na_2S_2O_4$ (10 mL, 1.8 M) in 10 mM NaOH was added to a sample of met-Lb (130 μL, ∼6.8 mM) after flushing each solution with Ar (20 min) (*20*). The deoxy-Lb solution (140 μL, ∼6.3 mM) was flushed with NO for 25 min after which the color had changed from blood red to brick red, characteristic of low-spin, six-coordinate heme proteins (*39*).

$Lb^{III}NO$ was obtained from met-Lb (130 μL, ∼8.4 mM) in KP_i (0.1 M, pH 7.0) buffer by flushing with Ar (20 min) and then NO (25 min). As soon as the met-Lb solution was exposed to NO, it was kept on ice to reduce the rate of "autoreduction".

Preparation of Protein Samples for XAFS. A sample vial containing glycerol (40% v/v, Aldrich, 99.5+%) was flushed with Ar (20 min) and then NO (10 min). Both sample and glycerol vials were transferred to a glovebag where the LbNO solution was syringed into the vial containing glycerol, and the mixtures were homogenized using a vortex. The Lb^{II}-NO (230 μL, ∼3.8 mM) and $Lb^{III}NO$ (220 μL, ∼3.4 mM) solutions were frozen ∼30 min and ∼1 h, respectively, after exposure to NO.

Lucite protein XAFS cells (140 μL, 23 × 2 × 3 mm) with 63.5-μm Mylar tape windows were cleaned by ultrasonication in EtOH (15−20 min), thoroughly rinsed with Milli-Q water, soaked overnight in Na_2EDTA solution, rinsed thoroughly with Milli-Q water, and finally rinsed with deoxygenated buffer in an Ar-filled glovebag. The Lb solutions were syringed into the XAFS cells, which were then sealed with high-vacuum silicone grease (Dow Corning) and snap-frozen in a liquid N_2/*n*-hexane slurry (178 K).

X-ray Absorption Spectroscopy (XAS) Measurements. XAS spectra were recorded at the Stanford Synchrotron Radiation Laboratory (SSRL) on the unfocused beamline 7−3 (3 GeV, 55−100 mA), using a Si(220) double-crystal monochromator detuned 50% at 8257 eV to reduce harmonic contamination. The temperature was maintained at 10 K using an Oxford Instruments continuous-flow liquid helium CF 1208 cryostat. The X-ray energy was calibrated using an Fe foil (first inflection point, 7111.2 eV) (*40*). Fluorescence spectra were collected using a Canberra 13-element Ge array detector (*41*)[3] and were averages of multiple scans. Each scan consisted of 51 data points in the preedge region 6785−7085 eV, 433 data points in the edge region 7085−7150 eV, and 288 data points in the XAFS region 7150−8257 eV.

[2] Appleby, C. A., personal communication, 1996.

[3] The data were obtained with a more modern detector, which could take up to 150 000 counts s^{-1}.

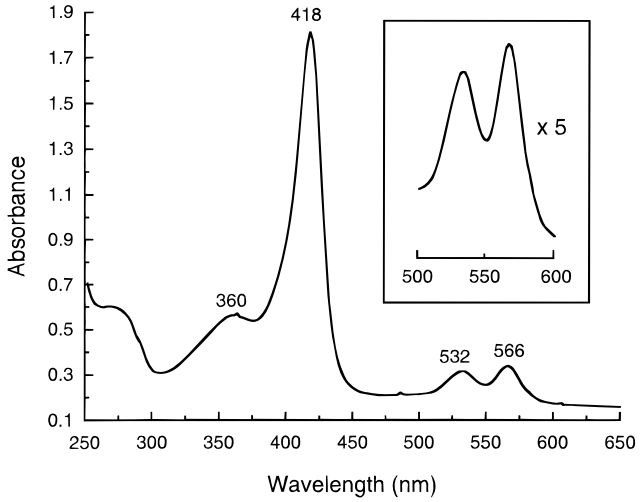

FIGURE 1: Electronic absorption spectrum of $Lb^{III}NO$ (~3 μM) for a solution in 40% aqueous glycerol (pH 7.0, 0.1 M KP_i) used in the XAFS experiment (3.4 mM) that had been diluted 1000-fold.

Photodecomposition of Protein Samples. During the Lb^{III}-NO data collection, the absorption edge shifted to lower energy, as a function of exposure time. To reduce this photodamage (i) two samples were used, and (ii) when the shifts in the edge became apparent, the beam was moved to a fresh "spot" on the sample. A total of 18 scans, consisting of 3−7 scans from two spots on each of two samples, were recorded.

Refinements (42). The XAFS data were analyzed using the program XFIT (*42*).[4] The bond length, bond angle, and other geometrical restraints applied to the model have been reported in detail elsewhere (*32*, *37*). A weight (*w*) value of 8 was applied to the XAFS data relative to the restraints, since this resulted in root-mean-square (rms) deviations between refined and ideal values of geometrical parameters close to the specified σ_{res} values. Monte Carlo error analyses were also performed as reported previously (*32*, *37*, *42*).

RESULTS

Preparation and Electronic Spectra of LbNO Adducts. The purity of the NO adduct used in the XAFS analysis was established from the electronic absorption spectrum of $Lb^{II}NO$ (*43*). Attempts at preparing $Lb^{II}NO$ by autoreduction of the $Lb^{III}NO$ adduct did not yield spectra characteristic of $Lb^{II}NO$ (prepared by reaction of deoxy-Lb with NO in the absence of O_2).

$Lb^{III}NO$ has not been reported previously, but samples can be prepared in a manner similar to $Mb^{III}NO$ (*37*). The electronic absorption spectrum of $Lb^{III}NO$ (Figure 1) is similar to that of the well-characterized $Mb^{III}NO$ (*39*). This, together with the X-ray absorption edge spectrum as compared to $Mb^{III}NO$ (see below), was used to show that the sample of $Lb^{III}NO$ was ≥90% pure.

Edge Spectra and Photodamage of LbNO. The XANES spectra of $Lb^{II}NO$ and $Lb^{III}NO$ are very similar to those of their MbNO analogues (Figure 2). During data collection from $Lb^{III}NO$, an edge shift to lower energy of up to 0.5 eV, compared to the first scan, was observed. This compares

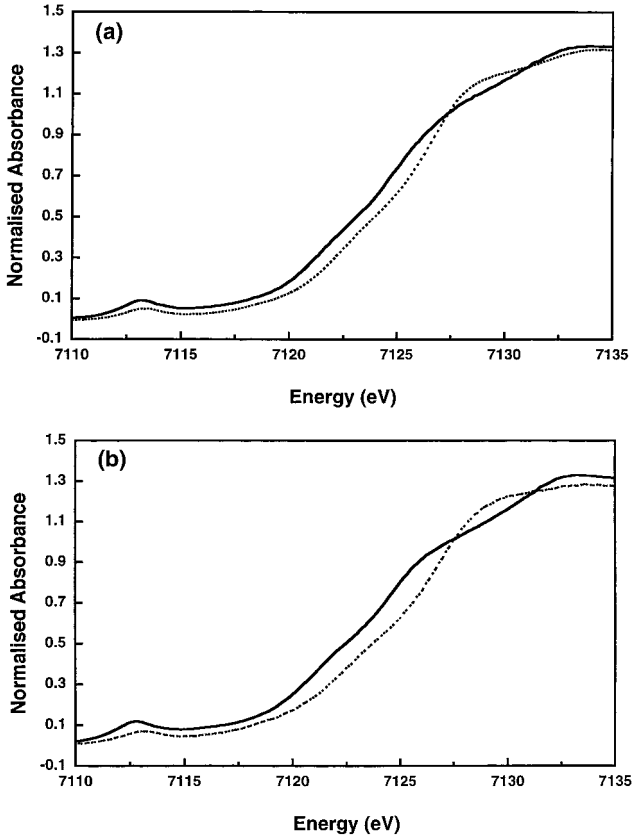

FIGURE 2: Edge spectra of (a) horse heart $Mb^{II}NO$ (—) as compared with $Mb^{III}NO$ (- - -) and (b) soybean $Lb^{II}NO$ (—) as compared with $Lb^{III}NO$ (- - -).

to a difference of 0.6 eV between the edges obtained from the first scans of $Lb^{II}NO$ and $Lb^{III}NO$. The XAFS model was fitted to the average of the 14 scans with edge shifts of less than 0.24 eV. As the edge shift $Lb^{II}NO$ was negligible (average shift 0.05 eV), all 22 scans were used.

MS XAFS of $Lb^{II}NO$ and $Lb^{III}NO$. The observed and calculated MS XAFS, the corresponding Fourier transforms, the residuals, the window functions used in the Fourier filter, and the refined Fe environments for $Lb^{II}NO$ and $Lb^{III}NO$ are shown in Figures 3−5, respectively. The Fe−N bond lengths and Fe−N−O bond angles together with the corresponding values from other XAFS and XRD analyses of ferrous and ferric nitrosyl proteins and complexes are summarized in Table 1. For $Lb^{II}NO$, the MS analysis gave $Fe-N_p$(av) as 2.02 Å, $Fe-N_\epsilon$ as 1.98 Å, $Fe-N_{NO}$ as 1.77 Å, and the Fe−N−O angle as 147° (R = 16.1%). The $Fe-N_p$(av) and $Fe-N_{NO}$ bond lengths are in good agreement with the X-ray crystal structures of [Fe(TPP)(NO)(1-MeIm)] (*44*), [Fe(TPP)(NO)] (*45*), [Fe(OEP)(NO)] (*46*), and $Lb^{II}NO$ (*9*, *10*) and the XAFS structure of [Fe(TPP)(NO)] (*37*). However, the $Fe-N_\epsilon$ bond distance determined from the MS analysis is considerably shorter than the corresponding XRD distances in both [Fe(TPP)(NO)(1-MeIm)] and $Lb^{II}NO$ (1.98 Å, cf. 2.180(4) and 2.20(7) Å).

The bond lengths and angles obtained from the MS analysis of $Lb^{III}NO$ are 2.00, 1.89, and 1.68 Å for $Fe-N_p$(av), $Fe-N_\epsilon$, and $Fe-N_{NO}$, respectively. The Fe−N−O angle was 173° (R = 18.2%). The $Fe-N_p$(av) and $Fe-N_{NO}$ bond lengths are similar to those determined from the X-ray crystal structures of $[Fe(TPP)(NO)(OH_2)]^+$ (*47*), $[Fe(OEP)(NO)]^+$ (*47*), and $[Fe(OEP)(NO)L]^+$ (*48*).

[4] This program incorporates FEFF 6.01 for MS [Rehr, J. J., Albers, R. C., and Zabinsky, S. I. (1992) *Phys. Rev. Lett. 69*, 3397−3400].

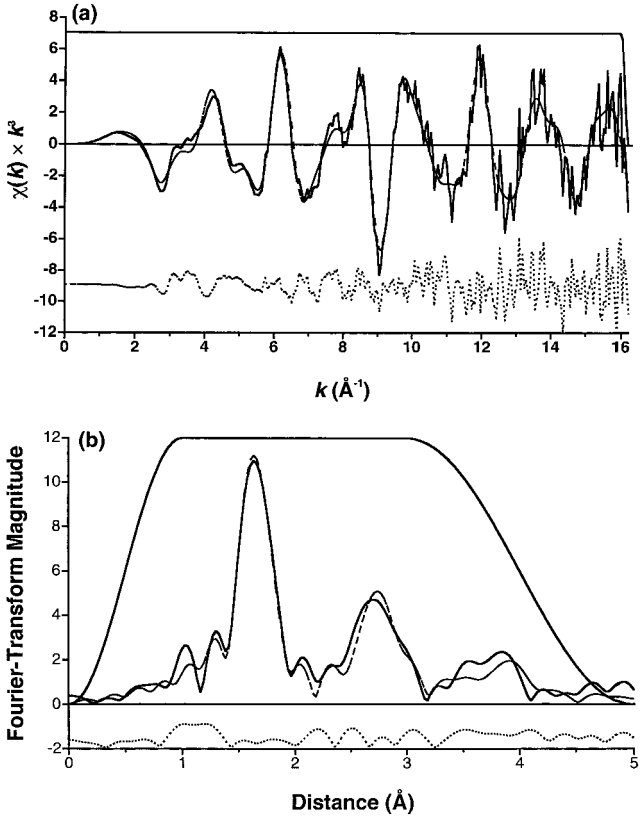

FIGURE 3: (a) XAFS and (b) Fourier transform amplitude of XAFS of soybean $Lb^{II}NO$: observed (—), calculated from refined model (- - -), residual (···), window used in Fourier filter (—).

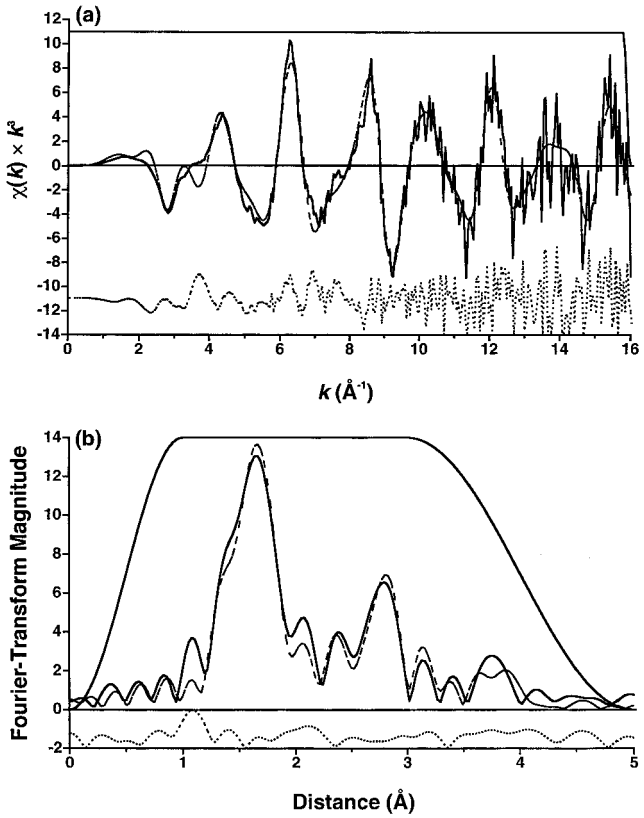

FIGURE 4: (a) XAFS and (b) Fourier transform amplitude of XAFS of soybean $Lb^{III}NO$: observed (—), calculated from refined model (- - -), residual (···), window used in Fourier filter (—).

Precision of the XAFS-Derived Parameters. A series of tests were conducted to investigate factors potentially limiting the precision of the XAFS-derived Fe−N distances and Fe−N−O angle. Specifically, the effects on the Fe−N−O angle of varying the restrained N−O distance by ±0.01 Å and of varying the Fe−N_ϵ distance over a range of approximately 0.5 Å were determined. The imprecision in the Fe−N distances and Fe−N−O angle arising out of noise in the data was also calculated.

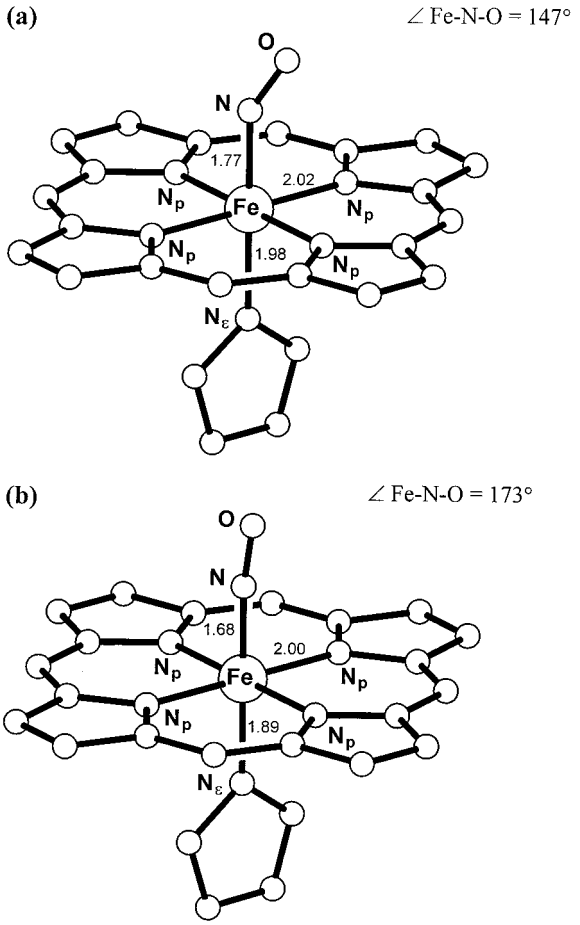

FIGURE 5: XAFS-derived molecular structures of the active sites of (a) $Lb^{II}NO$ and (b) $Lb^{III}NO$ at 10 K.

Effect of Varying the N−O Distance on the Fe−N−O Angle in $Lb^{II}NO$ and $Lb^{III}NO$. For the XAFS refinements, the N−O distance was restrained to a value of 1.12 Å taken from model compounds. To account for the uncertainty in this value, the effect on the Fe−N−O angle of a 0.01-Å change was determined. A variation of the restrained N−O distance in the refinement of $Lb^{II}NO$ by ±0.01 Å resulted in a variation of 2.5° in the Fe−N−O angle (Table S1). Hence, if the uncertainty in the N−O distance is 0.01 Å, then the consequent uncertainty in the Fe−N−O angle is approximately 1.3°. For $Lb^{III}NO$, the variation was 7.2°, corresponding to an uncertainty of approximately 3.6° in the Fe−N−O angle. These esd values were used in calculating the overall estimate of the rms error in ∠Fe−N−O.

Effect of Varying the Fe−N_ϵ Distance. Because the XAFS from the imidazole ring of the proximal histidine is expected to be similar to that from the four rings of the heme, but somewhat weaker, the Fe−N_ϵ bond distance is expected to be the least well determined of the Fe−N distances. To determine the effect of varying the Fe−N_ϵ bond length on the Fe−N−O angle and Fe−N_{NO} bond distance in soybean $Lb^{II}NO$, a series of refinements was conducted with the

Table 1: Comparison of Fe−Ligand Bond Lengths and Angles in $Lb^{II}NO$ and $Lb^{III}NO$ Obtained from MS XAFS Analyses with Those Determined from Other XAFS Analyses or X-ray Crystal Structure Data

		Fe−ligand distances (Å)				av Fe−N[a] (Å)	Fe−N−O angle (°)	Debye−Waller factors, σ^2 (Å^2)				other refinement parameters		
species	method	N_p	N_ϵ/OH_2/S	N_{NO}	N−O			N_p	N_ϵ	N_{NO}	O_{NO}	E_0(eV)	S_0^2	R(%)
$Lb^{II}NO$	MS[b]	2.02	1.98	1.77	1.12	2.01	147	0.003	0.001	0.002	0.007	7124.7	0.870	16.1
	crystal[c]	1.99(7)	2.20(7)	1.72(7)	1.35[d]	2.03	147(4)							18.4
$Mb^{II}NO$	MS[e]	1.99	2.05	1.76	1.12	2.00	150	0.002	0.001	0.005	0.005	7125.0	0.865	13.8
	crystal[f]	2.07_7	2.18(3)	1.89(4)	1.15	2.09_7	112							
$Hb^{II}NO$	crystal[g]			1.74	1.1		145(10)							
RSNO$Hb^{II}NO$	crystal[h]		2.28	1.74, 1.75	1.11, 1.13		123,131							18.4
Cyt *c* peroxidase (NO)	crystal[i]		2.04	1.82			125,135							
[Fe(TPP)(NO)]	crystal[j]	2.001(3)	-	1.717(7)	1.12(1)	2.00	149.2(6)							6.1
	MS[k]	2.00		1.73	1.12	2.00	156	0.003		0.005	0.007	7126.3	0.970	12.7
[Fe(OEP)(NO)]	crystal[l]	1.99−2.02		1.722(2)		2.00	144.4(2)							4.2
[Fe(OEP)(NO)]	crystal[l]	2.00−2.02		1.731(1)		2.01	142.7(1)							4.1
[Fe(TPP)(NO) (1-MeIm)]	crystal[m,n]	2.008(4)	2.180(4)	1.743(4)	1.121(8)	2.04	142.1(6)							7.4
					1.14(1)		138(1)							
$Lb^{III}NO$	MS[b]	2.00	1.89	1.68	1.12	1.98	173	0.001	0.001	0.004	0.008	7127.2	1.13	18.2
$Mb^{III}NO$	MS[o]	2.00	2.04	1.68	1.13	2.01	180	0.001	0.001	0.006	0.006	7128.8	0.946	14.3
P450nor-NO	MS[p]	2.00	2.26	1.66			170							
P450cam-NO	MS[p]	2.00	2.26	1.76			170							
[Fe(TPP)(NO) $(OH_2)]^+$	crystal[q,r]	1.999(6)	2.001(5)	1.652(5)	1.150	2.00	174(1)							7.9
[Fe(OEP) $(NO)]^+$	crystal[q,s]	1.994(3)	-	1.644(3)	1.112(4)	1.99	176.9(3)							6.3
[Fe(OEP) $(NO)L]^+$	crystal[t]	2.00	1.99−2.04	1.63−1.67		2.00	177							

[a] The average Fe−N distance includes the four Fe−N_p values and Fe−N_ϵ, if applicable. [b] This work; data were collected at 10 ± 1 K and were analyzed using the TPP model. [c] 1.8 Å resolution (*9*). The DPI value (*57*) for the structure was calculated to be 0.14 Å giving estimated errors in the Fe−L bond lengths of at least 0.2 Å. [d] The error estimate in L−L bond lengths is uncertain. [e] Data were refined with R_{max} = 5.1 Å (R_{eff} = 10.2 Å), number of legs = 6, and no filters ∴ 285 unique paths were examined and included in the refinement (*37*). [f] The sperm whale $Mb^{II}NO$ structure was refined to 1.7 Å (*30*); DPI value = 0.14 Å, therefore, there are considerable errors in both the bond lengths and the ∠Fe−N−O bond angle. [g] 2.8-Å resolution (*28*). The structure of horse $Hb^{II}NO$ was deduced by a difference Fourier map of HbNO minus met-Hb, calculated using the refined phases of met-Hb, [Ladner, R. C., Heidner, E. J., and Perutz, M. F. (1977) *J. Mol. Biol. 114*, 385−414]; hence, *R* was not reported. Error in Fe−N_{NO} bond length is estimated to be at least 0.2 Å. Deatherage and Moffat (*28*) estimate the error in ∠Fe−N−O to be ±10°. [h] Ref *29*. [i] Ref *31*. [j] Data were collected at 293 K (*45*). [k] Model included the α carbons of the phenyl substituents (*37*). [l] There are two different crystal structures (*46*). [m] Data were collected at 293 K (*44*). [n] The two bonds and angles represent the major and minor orientations of the nitrosyl oxygen. The occupancy factors of the oxygen atoms were 0.67(3) and 0.32(2), respectively. [o] 15-scan average. 105 unique paths included in the refinement. Errors in E_0 and S_0^2 were 0.2 eV and 0.014, respectively (*37*). [p] P450nor refers to the nitric oxide reductase (nor) enzyme from *Fusarium oxysporum*, which has been designated as a cytochrome P450 system because of its similarity to this class of enzymes. P450cam refers to the *d*-camphor-bound form of cytochrome P450 from *Pseudomonas putida* (*23*). [q] Ref *47*. [r] Data were collected at 96 K. [s] Data were collected at 292 K. [t] These are the average of several structures with L = 1-methylimidazole, pyrazole, indazole, or pyrazine (*48*).

Fe−N_ϵ bond fixed at distances between 1.95 and 2.30 Å in 0.05-Å increments. There were no significant changes in the resulting Fe−N_{NO} bond distance. The changes in the Fe−N−O bond angle ranged from +4° to −2° (Figure S1). The best refinement resulted from an Fe−N_ϵ bond distance of 2.00 Å (R = 15.9%). This is in good agreement with the Fe−N_ϵ bond distance obtained in the original refinement (1.98 Å). For $Lb^{III}NO$, when the Fe−N_ϵ bond distance was increased from 1.80 to 2.30 Å in 0.05-Å increments (Table S5), there was no significant change in the Fe−N_{NO} bond distance. The changes in the Fe−N−O bond angle ranged from +7° to −7° (Figure S1). As in the unconstrained refinement, the best refinement had an Fe−N_ϵ bond distance of 1.90 Å (R = 18.6%).

Imprecision Arising from Noise in the XAFS Data. Monte Carlo calculations of error due to noise in the data yielded respective rms errors for $Lb^{II}NO$ and $Lb^{III}NO$ of 0.002 and 0.003 Å for Fe−N_p, 0.009 and 0.012 Å for Fe−N_ϵ, and 0.004 and 0.006 Å for Fe−N_{NO}. The errors introduced by noise in the data are more significant for the Fe−N−O bond angle, for which the Monte Carlo calculations yielded rms errors of 3.0° and 5.3° for $Lb^{II}NO$ and $Lb^{III}NO$, respectively.

Combined Estimates of Precision. With the exception of the Fe−N_ϵ values, the errors in the Fe−N due to noise are small as compared to ±0.02 Å, the typical systematic error in XAFS analyses (*49*). Consequently, a precision of 0.02 Å was estimated for the Fe−N bond lengths.

The estimated errors in the Fe−N−O bond angle were obtained by combining the uncertainty due to the N−O restraint with that due to noise in the data. For $Lb^{II}NO$, combining the respective values of 3.0° and 1.3°, this yielded a final estimate of 3.3°.[5] For $Lb^{III}NO$, combining 5.3° with 3.6° yielded a final estimate of 5.5°. If the variation arising from changing the Fe−N_ϵ distance is also included, these values become approximately 5° and 9°, respectively. Just as in X-ray crystallography, these calculated errors may underestimate the true errors, although bond length data from a NO−Fe−porphyrin complex suggests that the errors in the Fe−N_{NO} and Fe−N_p distances are within this range (*37*).

[5] Estimate of rms error in the Fe−N−O angle for $Lb^{II}NO$: error in ∠Fe−N−O = $\sqrt{(1.3°)^2+(3.0°)^2}$ = 3.3°. Estimate of rms error in the Fe−N−O angle for $Lb^{III}NO$: error in ∠Fe−N−O = $\sqrt{(3.6°)^2+(4.1°)^2}$ = 5.5°.

To examine the sensitivity of the fit to the XAFS on the Fe−N−O angle, refinements were performed with a range of tightly restrained angles between 109° and 180° (σ_{res} = 1°) for $Lb^{II}NO$ and $Lb^{III}NO$. These restraints were then removed, and the data were re-refined (Tables S2 and S3). For $Lb^{II}NO$, two minima were observed; when the initial bond angle was 109°, the Fe−N−O angle refined to an unlikely angle of 102° after restraints were removed. For 120°, the angle refined to 150° after the restraints were removed, whereas for angles of 130° or higher, the Fe−N−O angle refined to a value of 147°. The *R* values for the minima where the Fe−N−O angle refined to a value of 102° or 150° are 3.5% and 2.6% higher, respectively, than where the angle refined to 147°. In the refinements including the Fe−N−O restraints, the Fe−N bond lengths did not deviate significantly from those of the best fit at 147°.

For $Lb^{III}NO$ there is only one minimum (173°) for starting angles ≥130°. When the restraints were removed for initial starting angles of 109° or 120°, the analyses refined to new minima with bond angles of 91° and 122°, respectively, but with higher *R* values. In the refinements incorporating the Fe−N−O restraints, the Fe−N bond lengths deviated by less than 0.02 Å.

As a final test, the Fe−N−O angle was restrained to values between 100° and 180°, and MS refinements were performed with an FT XAFS window including only the region most sensitive to the Fe−N−O angle (∼2.0−2.3 Å). The variations in *R* values illustrate the sensitivities of the data to this angle (Figure S2).

Degree of Determinancy and Alternative Methods of Error Analysis. The number of parameters being refined, *p*, as compared to the number of independent points, N_i, can be calculated to give the degree of determinancy N_i/p. If this ratio is less than 1, the fit is underdetermined and a unique fit is not possible, whereas a ratio above 1 gives an overdetermined problem, which can be used to give a unique fit. To ensure that the problem is overdetermined for heme proteins (*34*), constraints and restraints are required where the value of N_i is given by

$$N_i = 2(\Delta r)(\Delta k)/\pi + [\Sigma D(N - 2) + 1] \qquad (1)$$

where *D* is the number of dimensions in which the refinement takes place (2 for the planar porphyrin, imidazole, and NO units used in the analysis), and *N* is the number of atoms in the unit. The model used in these calculations together with the large *k*-range (16 $Å^{-1}$) of data used in the fit result in a well-overdetermined MS XAFS fit ($N_i/p = 1.7$). This is much better than those reported in the literature in the early 1990s (e.g., refs *33*−*35*), largely due to improvements in the sensitivity of detection of XAFS, which enables data to be collected and analyzed over a larger *k* range.

The values of N_i and *p* can also be used to calculate errors from the changes in the R^2 values when refinements are used with constrained bond lengths and angles around the minimum (*35*). Using such analyses the errors in the bond lengths and angles are similar to those estimated above (e.g., 0.03 Å in the $Fe-N_\epsilon$ bond, 7° in the Fe−N−O angle, and smaller errors in the Fe−NO and $Fe-N_p$ bond lengths).

DISCUSSION

Characterization and Properties of $Lb^{III}NO$. The interest in LbNO stems from its potential important biological roles (*3*, *7*). While $Lb^{II}NO$ is well-characterized, $Lb^{III}NO$ has not been reported. The preparation of the latter is the same as that used for $Mb^{III}NO$, and its identity has been established by the similarity of its electronic absorption and XAS spectra and XAFS with those of the well-characterized $Mb^{III}NO$ (*37*). $Lb^{III}NO$ is more sensitive to denaturation than $Mb^{III}NO$, as indicated by the greater sensitivity to autoreduction and photoreduction of the Lb adduct, and the observation that the autoreduction of $Mb^{III}NO$ in the presence of excess NO does not result in denaturation. Nonetheless, with care in the handling of the $Lb^{III}NO$ adduct and careful monitoring of photodamage, good XAS data were obtained at 10 K.

Comparisons between MbNO and LbNO. The use of restrained and constrained refinements in the XAFS analysis of heme proteins is well-established (*33*, *34*). In the present case, the bond lengths and bond angles of the heme group and the imidazole were restrained to remain within the normal variations found in model complexes (*32*, *37*), and symmetry and other constraints were applied to further limit the number of variables that are free to refine. This combined with the large *k* range results in a well-determined fit to the XAFS as compared with previous work on heme proteins (*33*−*35*). The reliability of this approach has been demonstrated by the excellent correspondence between the MS XAFS-derived structures (*32*) and the recently published X-ray structures of deoxy and met-Mb at ∼1-Å resolution (*50*, *51*) and its ability to reproduce accurately the bond lengths in the model complex, [Fe(TPP)(NO)] (*37*). While the XAFS-derived bond angle determined for this structure was 7° larger than that derived by X-ray crystallography, the discrepancy may be an artifact of the 4-fold disorder of the NO group in the crystal structure. For structures of NO adducts of Fe−porphyrins, where there is no disorder, there is a tilt of 6−8° of the NO group from the plane perpendicular to the porphyrin (*46*). As the authors point out, it was evident that all previous structures of such porphyrin complexes had a similar tilt, which was not evident in the crystal structure of [Fe(TPP)(NO)] because of the 4-fold disorder, except for the large temperature factors of the NO nitrogen (*45*). Such a tilt in the crystal structure of [Fe(TPP)(NO)] would result in the XAFS-derived angle being identical to the XRD-derived angle. Taken together, these establish that our model has been able to reproduce accurately bond lengths and angles in related systems. This gives us considerable confidence in the XAFS-derived parameters for $Lb^{II}NO$ and $Lb^{III}NO$.

In the calculations described here, the bonding variables that are free to change are the three Fe−ligand bond lengths and the Fe−N−O bond angle. If the Fe−N−O moiety in MbNO and LbNO is nearly linear, MS effects are very important (*52*). Under these conditions, the XAFS amplitude enhancement due to the forward scattering, or "focusing", of the photoelectron by the intervening N atom can be as large as a factor of 10 (*52*). Such MS effects are important for absorber−scatterer−scatterer angles between 150° and 180°, as in the nitrosyl adducts of heme proteins, where MS involving 2-, 3-, and 4-leg paths are all major contributions for the Fe−N−O moiety (*32*). As a result, the MS analyses can distinguish between bent and linear geometries. Because the NO ligand is also substantially closer to the Fe atom than the other ligands, the MS XAFS analyses are able to determine the Fe−N−O angle in ferrous and ferric nitrosyl

Mb and Lb, despite the large MS contributions from the heme group.[6] This is reflected in the region of the second shell (Figures 3 and 4), where the observed and calculated FT of the XAFS for the two LbNO proteins are quite different. This analysis has been outlined in detail for the MbNO proteins (*37*) and will not be reiterated here. From these results and those reported in the literature, it is clear that the Fe−N−O angle is bent in ferrous LbNO, while in the ferric nitrosyl complex, the angle is close to being linear.

The $Fe-N_p$, $Fe-N_\epsilon$, and $Fe-N_{NO}$ bond lengths and Fe−N−O angles determined from MS XAFS of horse heart MbNO and soybean LbNO are similar (Table 1). In both MbNO and LbNO, the $Fe-N_p$ and $Fe-N_{NO}$ bond lengths are the same, within the error of the analyses. However, the $Fe-N_\epsilon$ bond lengths in ferrous and ferric LbNO are somewhat shorter than in the corresponding Mb adducts (1.98 and 1.89 Å in $Lb^{II}NO$ and $Lb^{III}NO$, respectively; cf. 2.05 and 2.04 Å for $Mb^{II}NO$ and $Mb^{III}NO$, respectively). The Fe−N−O bond angles are not significantly different in analogous LbNO and MbNO adducts, (147° and 173° in $Lb^{II}NO$ and $Lb^{III}NO$; cf. 150° and 180° in $Mb^{II}NO$ and $Mb^{III}NO$).

The stronger ligand fields of the Lb proteins evident from the positions of the edges (higher energies for the Lb complexes as compared to their Mb analogues) in this work has been attributed to ruffling of the porphyrin ring in RR studies (*16, 17*). As it has been previously shown that ruffling the heme group in met-Lb has little effect on the MS XAFS (*53*), no such models were used in the present analyses.

Comparisons between XAFS and Other Techniques. The similarity in the bond angles for $Mb^{II}NO$ and $Lb^{II}NO$ obtained from XAFS is in strong contrast with the dissimilarity of those obtained from X-ray crystallography, where they were determined to be 112° and 150°, respectively. As discussed previously (*32*), the discrepancy between the XAFS results for $Mb^{II}NO$ and the XRD and EPR results ($\angle$Fe−N−O = 108−110° at 77 K) (*54*−*56*) appears to arise from different methods of preparation. While normally the agreement between solution structures (NMR) and crystal structures of proteins is very good, this does not necessarily apply to the crystals of $Mb^{II}NO$ used in the EPR and XRD experiments, which required two chemical transformations after diffusion of NO into preformed crystals of met-Mb. In such preparations, the distal histidine of met-Mb in the crystals may block the NO from binding in the preferred angle found in model complexes (*44*−*46*), and it is possible that crystal packing forces and/or incomplete reaction results in different bond angles, whereas the samples used for the XAFS measurements were prepared directly in solution. The importance of packing forces in influencing the conformational changes required to move the distal histidine has been demonstrated in XRD studies, where the angle obtained for the binding of small molecules into crystals of hemes is sensitive to the packing forces within the crystal (*30*). An X-ray crystallographic study of horse HbNO also deduced an Fe−N−O bond angle of 145 ± 10° (*28*), which is the same, within experimental error, as the angle determined by XAFS for horse heart $Mb^{II}NO$ (*37*) and by XRD (*9*) and XAFS for $Lb^{II}NO$ but much larger than those observed in the XRD of RSNO−$Hb^{II}NO$ (*29*). It appears that in solution the NO adducts of all of the heme proteins adopt geometries that are consistent with simple model complexes (Table 1), irrespective of crowding in the heme pocket by the distal histidine.

In the XRD structure of lupin $Lb^{II}NO$ at 1.8 Å resolution (*9*), it was reported that "... the strong $Fe-N_{NO}$ bond (1.7 Å) leads to a slight lengthening of the Fe−His residue bond (2.2 Å) in comparison with other liganded Lbs ...". This is significantly longer than the $Fe-N_\epsilon$ bond length of 1.98 Å determined from our MS analysis of soybean *a* $Lb^{II}NO$. It is not clear whether this difference is due to the different method of preparation (solution for the XAFS versus crystal for the XRD), the packing forces, or the low precision of the XRD-derived bond lengths. The DPI calculation (*57*) shows that the average uncertainty in the atomic positions is 0.14 Å, so that the XRD and XAS structures are the same within the limited precision of the XRD result (Table 1).

In the absence of distal steric hindrance, the six valence electrons (metal *d* and ligand π^*) are expected to result in a linear $Fe^{III}-N-O$ linkage (*58*). FTIR studies of heme cd_1 nitrite reductase (*59*) have established that the ferric nitrosyl complex consists of "... a linear Fe−N−O unit in which substantial donation of charge from NO to Fe^{3+} occurs, resulting in a species with considerable NO^+ character ...". The MS XAFS analyses of the $Mb^{III}NO$ and $Lb^{III}NO$ are consistent with a linear Fe−N−O angle ($\angle$Fe−N−O ∼ 180°) found in other heme proteins and the model complexes (Table 1) and may be best described as $Fe^{II}NO^+$ adducts. Despite this, the positions of the edges in the XAS of the NO adducts of the two oxidation states establish that the $Fe^{II}NO^+$ adducts have a somewhat greater Fe(III) character than the $Fe^{II}NO$ proteins.

NO binds to the heme Fe of soluble guanylyl cyclase (sGC) to form a transient six-coordinate heme (*60*−*62*). In this complex, however, the Fe−His bond is unstable, and the breakage of this bond is involved in activation of the enzyme (*63*). The MS XAFS analyses of the ferric and ferrous nitrosyl adducts of horse heart Mb and soybean Lb do not indicate a weakening or breakage in this Fe−His bond. Clearly, some other factors are at play in weakening this bond in the NO adduct of sGC, which are not evident in the Lb and Mb proteins (Table 1). Finally, the strong bonding of NO in $Lb^{II}NO$ is consistent with its putative biological role in controlling nitrogen fixation.

CONCLUSIONS

The $Lb^{III}NO$ adduct has been prepared and characterized for the first time. Its spectral properties are similar to those of $Mb^{III}NO$, although it is somewhat more susceptible to reduction and denaturation.

The differences previously deduced between the Fe−N−O bond angles in $Lb^{II}NO$, $Hb^{II}NO$, and $Mb^{II}NO$ are not apparent in the MS XAFS analyses and may be artifacts of the method by which these adducts were generated for the single crystal studies. This implies that steric effects of the

[6] The importance of these NO multiple-scattering pathways is evident by the fact that, even for an Fe−N−O angle of 147° in $Lb^{II}NO$, the contributions to the XAFS for the 3-leg Fe→N→O→Fe path is 50% of the 3-leg paths of the iron porphyrin. For the 4-leg Fe→N→O→N→Fe path, this MS contribution is as large as for the 8-fold degenerate 4-leg path in the porphyrin. Since these are among the most important MS pathways, it is clear how the short bonds and larger angle in the Fe−NO moiety enable it to be distinguished from the porphyrin group, even in the adducts in which the moiety is bent.

distal histidine in Mb adducts are not as important as previously suggested, when the NO adducts are prepared in solution. The best estimates of errors in bond lengths in the published XRD structures, e.g., the DPI (Table 1) (*57*), are an order of magnitude higher than for the MS XAFS analyses. This, no doubt, is also a factor contributing to the apparent discrepancies.

ACKNOWLEDGMENT

We would like to thank SSRL for access to the facilities, Professor K. Hodgson and Dr. Britt Hedman for assistance at SSRL and discussion of the results, Dr. C. A. Appleby for assistance with manipulations of Lb *a* and helpful discussions, and Professor H. C. Freeman and Dr. A. Levina for helpful discussions.

SUPPORTING INFORMATION AVAILABLE

Tables (S1−S5) of the effects of restraining the Fe−N−O bond angle and the N−O or Fe−N_ϵ bond lengths on the MS XAFS analyses of LbNO (7 pages). This material is available free of charge via the Internet at http://pubs.acs.org.

REFERENCES

1. Appleby, C. A. (1974) in *The Biology of Nitrogen Fixation* (Quispel, A., Ed.) pp 521−554, North-Holland, Amsterdam.
2. Appleby, C. A. (1984) *Annu. Rev. Plant Physiol. 35*, 443−478.
3. Fuchsman, W. H. (1992) *Adv. Comp. Environ. Physiol. 13*, 23−57.
4. Martin, K. D., Saari, L., Guang-Xin, W., Wang, T., Parkhurst, L. J., and Klucas, R. V. (1990) *J. Biol. Chem. 265*, 19588−19593.
5. Ellfolk, N. (1961) *Acta Chem. Scand. 15*, 975−984.
6. Appleby, C. A., Wittenberg, B. A., and Wittenberg, J. B. (1973) *Proc. Natl. Acad. Sci. U.S.A. 70*, 564−568.
7. Narula, S. S., Dalvit, C., Appleby, C. A., and Wright, P. E. (1988) *Eur. J. Biochem. 178*, 419−435.
8. Harutyunyan, E. H., Safonova, T. N., Kuranova, I. P., Popov, A. N., Teplyakov, A. V., Obmolova, G. V., Rusakov, A. A., Vainshtein, B. K., Dodson, G. G., Wilson, J. C., and Perutz, M. F. (1995) *J. Mol. Biol. 251*, 104−115.
9. Harutyunyan, E. H., Safonova, T. N., Kuranova, I. P., Popov, A. N., Teplyakov, A. V., Obmolova, G. V., Vainshtein, B. K., Dodson, G. G., and Wilson, J. C. (1996) *J. Mol. Biol. 264*, 152−161.
10. Obmolova, G. V., Safonova, T. N., Teplyakov, A. V., Popov, A. N., Kuranova, I. P., Harutyunyan, E. G., and Vainshtein, B. K. (1988) *Bioorg. Khim. 14*, 1509−1519.
11. Appleby, C. A., Nicola, N. A., Hurrell, J. G. R., and Leach, S. J. (1975) *Biochemistry 14*, 4444−4450.
12. Andersson, C. R., Jensen, E. O., Llewellyn, D. J., Dennis, E. S., and Peacock, W. J. (1996) *Proc. Natl. Acad. Sci. U.S.A. 93*, 5682−5687.
13. Fuchsman, W. H., and Appleby, C. A. (1979) *Biochim. Biophys. Acta 579*, 314−324.
14. Maskall, C. S., Gibson, J. F., and Dart, P. J. (1977) *Biochem. J. 167*, 435−445.
15. Kanayama, Y., and Yamamoto, Y. (1990) *Plant Cell Physiol. 31*, 207−214.
16. Armstrong, R. S., Irwin, M. J., and Wright, P. E. (1980) *Biochem. Biophys. Res. Commun. 95*, 682−689.
17. Trewhella, J., and Wright, P. E. (1980) *Biochim. Biophys. Acta 625*, 202−220.
18. Armstrong, R. S., Irwin, M. J., Wellington, J. E., and Wright, P. E. (1982) *Acta Chem. Scand. B36*, 263−265.
19. Irwin, M. J. (1982) Ph.D. Thesis, University of Sydney.
20. Irwin, M. J., Armstrong, R. S., and Wright, P. E. (1981) *FEBS Lett. 133*, 239−243.
21. Benko, B., and Yu, N.-T. (1983) *Proc. Natl. Acad. Sci. U.S.A. 80*, 7042−7046.
22. Eich, R. F., Li, T., Lemon, D. D., Doherty, D. H., Curry, S. R., Aitken, J. F., Mathews, A. J., Johnson, K. A., Smith, R. D., Phillips, G. N., Jr., and Olson, J. S. (1996) *Biochemistry 35*, 6976−6983.
23. Obayashi, E., Tsukamoto, K., Adachi, S.-i., Takahashi, S., Nomura, M., Iizuka, T., Shoun, H., and Shiro, Y. (1997) *J. Am. Chem. Soc. 119*, 7807−7816.
24. Owens, J. W., and O'Connor, C. J. (1988) *Coord. Chem. Rev. 84*, 1−45.
25. Stong, J. D., Burke, J. M., Daly, P., Wright, P., and Spiro, T. G. (1980) *J. Am. Chem. Soc. 102*, 5815−5819.
26. Walters, M. A., and Spiro, T. G. (1982) *Biochemistry 21*, 6989−6995.
27. Zhang, K., Reddy, K. S., Bunker, G., and Chance, B. (1991) *Proteins: Struct. Funct. Genet. 10*, 279−286.
28. Deatherage, J. F., and Moffat, K. (1979) *J. Mol. Biol. 134*, 401−417.
29. Chan, N. L., Rogers, P. H., and Arnone, A. (1998) *Biochemistry 37*, 16459−16464.
30. Brucker, E. A., Olson, J. S., Ikeda-Saito, M., and Phillips, G. N., Jr. (1998) *Proteins: Struct. Funct. Genet. 30*, 352−356.
31. Edwards, S. L., and Poulos, T. L. (1990) *J. Mol. Biol. 265*, 2588−2595.
32. Rich, A. M., Armstrong, R. S., Ellis, P. J., Freeman, H. C., and Lay, P. A. (1998) *Inorg. Chem. 37*, 5743−5753.
33. Hasnain, S. S., and Strange, R. W. (1990) *Biophysics and Synchrotron Radiation* (Hasnain, S. S., Ed.), Chapter 4, Ellis Horwood Ltd., Chichester, U.K.
34. Binsted, N., Strange, R. W., and Hasnain, S. S. (1992) *Biochemistry 31*, 12117−12125.
35. Chance, M. R., Miller, L. M., Fischetti, R. F., Scheuring, E., Hunag, W.-X., Sclavi, B., and Sullivan, M. (1996) *Biochemistry 35*, 9014−9023.
36. Westre, T. E., Cicco, A. D., Filipponi, A., Natoli, C. R., Hedman, B., Solomon, E. I., and Hodgson, K. O. (1994) *J. Am. Chem. Soc. 116*, 6757−6768.
37. Rich, A. M., Armstrong, R. S., Ellis, P. J., and Lay, P. A. (1998) *J. Am. Chem. Soc. 120*, 10827−10836.
38. Rassmussen, P. J. (1986) B.Sc. (Hons) Thesis, University of Sydney.
39. Addison, A. W., and Stephanos, J. J. (1986) *Biochemistry 25*, 4104−4113.
40. Zhang, Y., Pavlosky, M. A., Brown, C. A., Westre, T. E., Hedman, B., Hodgson, K. O., and Solomon, E. I. (1992) *J. Am. Chem. Soc. 114*, 9189−9191.
41. Cramer, S. P., Tench, O., Yocum, M., and George, G. N. (1988) *Nucl. Instrum. Methods Phys. Res. A266*, 586−591.
42. Ellis, P. J., and Freeman, H. C. (1995) *J. Synchrotron Radiat. 2*, 190−195.
43. Antonini, E. (1965) *Physiol. Rev. 45*, 123−170.
44. Scheidt, W. R., and Piciulo, P. L. (1976) *J. Am. Chem. Soc. 98*, 1913−1919.
45. Scheidt, W. R., and Frisse, M. E. (1975) *J. Am. Chem. Soc. 97*, 17−21.
46. Ellison, M. K., and Scheidt, W. R. (1997) *J. Am. Chem. Soc. 119*, 7404−7405.
47. Scheidt, W. R., Lee, Y. J., and Hatano, K. (1984) *J. Am. Chem. Soc. 106*, 3191−3198.
48. Ellison, M. K., and Scheidt, W. R. (1999) *J. Am. Chem. Soc. 121*, 5210−5219.
49. Gurman, S. J. (1995) *J. Synchrotron Radiat. 2*, 56−63.
50. Kachalova, G. S., Popov, A. N., and Bartunik, H. D. (1999) *Science 284*, 473−476.
51. Vojtěchovský, J.; Chu, K.; Berendzen, J.; Sweet, R. M., and Schlichting, I. (1999) *Biophys. J. 77*, 2153−2174.
52. Penner-Hahn, J. E., and Hodgson, K. O. (1989) in *Iron Porphyrins, Part III* (Lever, A. B. P., and Gray, H. B., Eds.) Vol. 4, Chapter 3, VCH Publishers, New York.
53. Rich, A. M. (1997), Ph.D. Thesis, University of Sydney.
54. Chien, J. C. W. (1969) *J. Chem. Phys. 51*, 4220−4227.
55. Dickinson, L. C., and Chien, J. C. W. (1971) *J. Am. Chem. Soc. 93*, 5036−5040.

56. Hori, H., Ikeda-Saito, M., and Yonetani, T. (1981) *J. Biol. Chem. 256*, 7849−7855.
57. Cruickshank, D. W. L. (1996) In *Macromolecular Refinement. Proceedings of the CCP4 Study Weekend, January 1996* (Dodson, E., Moore, M., Ralph, A., and Bailey, S., Eds.) pp 11−22, SERC Daresbury Laboratory, Warrington, U.K.
58. Yu, N.-T., and Kerr, E. A. (1988) in *Biological Applications of Raman Spectroscopy* (Spiro, T. G., Ed.) Vol. III, pp 39−95, John Wiley and Sons, New York.
59. Wang, Y., and Averill, B. A. (1996) *J. Am. Chem. Soc. 118*, 3972−3973.
60. Deinum, G., Stone, J. R., Babcock, G. T., and Marletta, M. A. (1996) *Biochemistry 35*, 1540−1547.
61. Stone, J. R., Sands, R. H., Dunham, W. R., and Marletta, M. A. (1995) *Biochem. Biophys. Res. Commun. 207*, 572−577.
62. Stone, J. R., and Marletta, M. A. (1996) *Biochemistry 35*, 1093−1099.
63. Kim, S., Deinum, G., Gardner, M. T., Marletta, M. A., and Babcock, G. T. (1996) *J. Am. Chem. Soc. 118*, 8769−8770.

BI990730N